Validating Granular Scaling Laws for Wheel/Screw Geometries

by

Teresa Mcbryan

A Thesis Presented in Partial Fulfillment
of the Requirements for the Degree
Master of Science

Approved April 2022 by the
Graduate Supervisory Committee:

Hamidreza Marvi, Chair
Spring Berman
Hyunglae Lee

ARIZONA STATE UNIVERSITY

May 2022

ABSTRACT

Building and optimizing a design for deformable media can be extremely costly. However, granular scaling laws enable the ability to predict system velocity and mobility power consumption by testing at a smaller scale in the same environment. The validity of the granular scaling laws for arbitrarily shaped wheels and screws were evaluated in materials like silica sand and BP-1, a lunar simulant. Different wheel geometries, such as non-grousered and straight and bihelically grousered wheels were created and tested using 3D printed technologies. Using the granular scaling laws and the empirical data from initial experiments, power and velocity were predicted for a larger scaled version then experimentally validated on a dynamic mobility platform. Working with granular media has high variability in material properties depending on initial environmental conditions, so particular emphasis was placed on consistency in the testing methodology. Through experiments, these scaling laws have been validated with defined use cases and limitations.

DEDICATION

This thesis is dedicated to my family and friends who supported me throughout all these years. I couldn't have done it without you. I especially want to thank my parents Pam and Bernie McBryan and Sarah McBryan, truly the greatest of all my siblings, for supporting me and inspiring me to reach for the stars. I also want to thank all my family and friends for keeping me sane during these past few difficult years, especially my fencing coach Florin Paunescu, the firepit Friday crew, and my NASAmigos.

ACKNOWLEDGMENTS

I want to thank the BIRTH (Bio-Inspired Robotics Technology and Healthcare) Lab and Professor Hamidreza Marvi for enabling this research. I want to especially acknowledge and thank the space mobility team within BIRTH Lab which includes Andrew Thoesen, Darwin Mick, Marko Green, and Justin Martia for being a great research team and guiding me throughout my research/schooling/life.

TABLE OF CONTENTS

Page

LIST OF TABLES

LIST OF FIGURES

Figure Page

CHAPTER 1

INTRODUCTION

For both Earth and space applications, understanding how vehicles move in granular media is important for creating optimal and robust robotic designs. Granular media are common materials that we see in everyday life, e.g. sand, powder, snow, etc. Despite decades of research, the physics of these media are still poorly understood and defined. They can behave as both a solid and fluid. This makes understanding and characterizing mobility of a system through this environment a very complex and difficult problem. Typical materials discussed through this thesis will include silica sand and BP-1, a type of lunar simulant. Particle size, angularity, porosity, and many other properties of granular media have high impact on the macroscopic behavior and, in turn, affects system behavior and overall mobility. This section will review properties of granular media and current leading theories that characterize and predict behavior of a dynamic system moving through these environments. Screw propelled vehicles are an alternative mobility method that works effectively in granular media.

1.1 What is Granular Media?

Granular media are composed of discrete solid macroscopic particles. They take on different physical properties that are typically attributed to different matter states: they flow as if liquids, can compress similar to gasses, and, like solids, can retain their shape independent of their environment or container [1].

The consistency and behavior depend on properties of the material and which flow regime it is following: rapid flow, quasi-static, and/or transitional. The particle behavior of the quasi-static regime is primarily influenced by the friction between particles according to Coulomb's friction law, with the rubbing and rolling of particle-on-particle causing momentum exchange. The rapid flow regime occurs when the particles are agitated, resulting in a fluidized behavior. In this case, the particles collide in short, binary collisions similar to a liquid or gas. In between these regimes is the state of transitional flow; not clearly defined [2]. For robotic mobility, the quasi-static and transitional regimes are the most common: quasi-static for undisturbed media and transitional as the system interacts with the environment. Properties of the material affect the media behavior in these flows as well as when the regime transitions. Factors such as particle size, angularity, porosity all affect how the granular media will behave. This research focuses on two main types of media: BP-1 and silica sand.

1.1.1 BP-1

BP-1, or Black-Point 1, is a lunar analogue found in the San Francisco Volcanic Field in northern Arizona. It originated as a byproduct from mining; however, NASA has conducted a detailed geotechnical assessment and has determined that its characteristics are similar to lunar regolith [3]. This lunar analogue can be used to simulate how vehicles would interact with the lunar surface leading to robust rover design and advancements in mining and excavation capabilities.

For the purpose of this thesis, the most significant characteristics of this media is that these particles are extremely fine: with 60% of particles <110 microns and 30% <55

microns. Additionally, the particle shape is classified as angular to sub-angular with an internal friction angle of 39-51º depending on the density which is higher angularity compared to most other lunar analogues. This can cause an almost cohesive-like effect to occur as the highly angular geometry make the particles effectively lock together with their high inter-particle frictional forces [3, 4, 5].

1.1.2 Silica Sand

Silica sand, also known as quikrete, is a well-characterized granular media used commonly (e.g. volleyball court grounds) and in research settings. Due to its popularity, silica sand is a highly accessible material. By using this common material, designs across different research groups and projects have reduced variability and study results can be directly compared and evaluated. For the purpose of this thesis, the most important characteristics is that the particles are primarily 0.3-0.8mm in size [6 , 7, 8]. The particle shape is considered “fairly round”, non-angular, and therefore does not have the same behavior that BP-1 exhibits.

1.2 Modeling Granular Media

The behavior of these media are difficult to capture. There are two main approaches to modeling granular media: continuum and discrete [1]. The continuum approach focuses on the macroscopic behavior and includes resistive force theory. While the discrete focuses on microscopic behavior which, in turn, affects macroscopic.

1.2.1 Resistive Force Theory

Resistive Force Theory (RFT) was originally used to model movement in fluids; however, it has demonstrated applicability in granular media as well. It breaks the intruding geometry like a wheel or screw into smaller and smaller segments which has an associated thrust and drag. Using linear superposition of forces, the thrust and drag are added up to predict overall characteristics of the system such as velocity and power. The predictive capabilities of this method are more effective if the media state is in the rapid-flow regime (also known as frictional fluid regime) and not applicable to cohesive media [9].

This theory has been experimentally validated for many use cases [10, 11, 12, 13], but does not accurately capture the characteristics of a screw moving through granular media as a screw contradicts the initial assumption that RFT must have non-disruptive flow [4].

1.2.2 Granular Scaling Laws Overview

Using intrusion forces from RFT, a scaled relationship between driving parameters and overall system dynamics was derived to find the granular scaling laws (GSL). These laws were first derived and tested using DEM simulations and experimental testing using a general wheel on a gantry [14, 15]. GSL are derived using non-dimensional analysis and empirical data from experiments/simulations to predict overall system characteristics such as steady state translational velocity and power draw. Initial validation and verification of these scaling laws demonstrate effective predictive

capability in ideal Coulombic materials. This research explores the application of these GSL on dynamic mobility systems.

1.2.3 Discrete Element Modelling (DEM)

With the rise in computational power, discrete element modelling has become a more and more common means of investigating behavior in granular media. DEM is effective at simulating individual particles and modelling interactions such as particle-on-particle and particle-on-intruding geometries. Both open sourced and commercial products have been created to process these simulations such as EDEM, LIGGGHTS, and LAMMPS [14, 15, 16, 17, 18, 19]. However, the complexity of simulations requires high computational capabilities and long run times, sometimes taking days to run a few seconds of simulation time. This makes modelling large systems impractical and costly. In order to reduce simulation run time, GSL can be combined with DEM. This combination results in comprehensive modelling of a smaller, scaled down, version of a system.

1.3 Screw Propelled Vehicles

Screw-propelled vehicles (SPVs) represent another mode of mobility over traditional wheels and offer benefits in difficult terrains. They utilize the rotation of auger-like cylinders to interact with the granular media to propel the system forward. Examples of SPVs include the Marsh Screw Amphibian, the Amphirol, and the Snowbird-6 that can traverse complex terrains such as mud, sticky clay, and water-ice

areas [20, 21, 22, 23]. For traditional wheeled crafts, these environments are nearly impossible to traverse without risk of getting stuck.

Screw propulsion represents an interesting mode of transportation, especially for space application. SPVs are being researched for application for lunar/asteroid rover designs in low-gravity environments. Traditional wheels depend on tractive force to move the system forward; however, that tractive force is affected by the normal force. Low gravity means this normal force is reduced, which can lead to potential slippage. Screw propelled vehicles represent a valid alternative solution to this problem.

CHAPTER 2

SYSTEM DEVELOPMENT LIFECYCLE

The purpose of this research was to create a system to validate granular scaling laws for both wheels and helical geometries in granular media. In order to achieve this goal, experimental designs were optimized for fast reproducibility for different types and sizes of intruder geometries. Over 1000 experimental test runs were successfully conducted. This chapter will go over the effects of intruder geometries and the system development lifecycle (SDLC) from its conceptual stages to implementation and testing.

2.1 Understanding Effect of Intruder Geometry

Insight into the terramechanics between the intruding geometry and granular media lead to optimal wheel design and advancements in robotic mobility. This research focuses on the wheel-soil interaction for non-grousered, straight-grousered, and bihelical-grousered wheels, and helicoid screws.

Grousers are protrusions on the wheel that increase traction in loose material by increasing contact area with the ground, shearing the volume of particles that the protrusion encounters. This strategy increases traction but conversely increases wheel sinkage and potential slippage. Typical grouser types, e.g. parallel, slanted, v-shaped (also known as chevron), and offset v-shaped, were empirically tested on a single wheeled gantry system and on a four wheeled dynamic mobility platform [24].

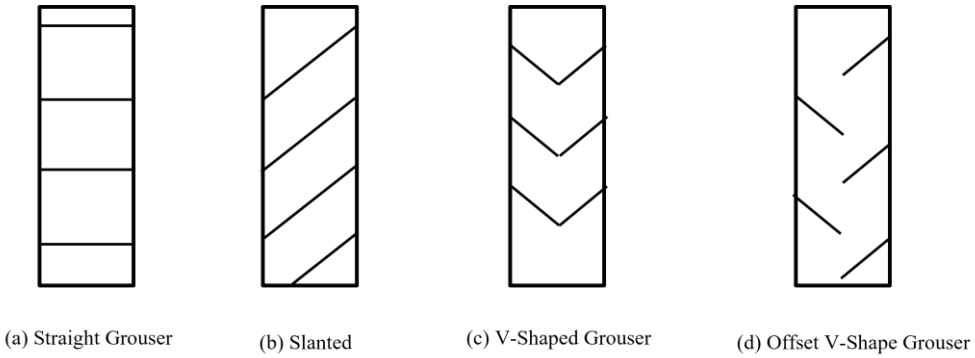

Figure 1. Basic Grouser Geometries in Planar View

Slip ratio, sinkage, driving torque, and traction load are key metrics used to determine wheel performance. As traction load increases, the slip ratio and wheel sinkage increase. The grouser shape does not greatly impact the sinkage at low slippage values. However, as the slip ratio increases above 40%, the digging and pushing of the subsoil is heavily influenced by grouser shape. For example, the geometry of the offset V-shaped grouser causes the displaced soil to exit at the grouser openings. Compared to the different grouser types, this shape leads to the largest sinkage [24].

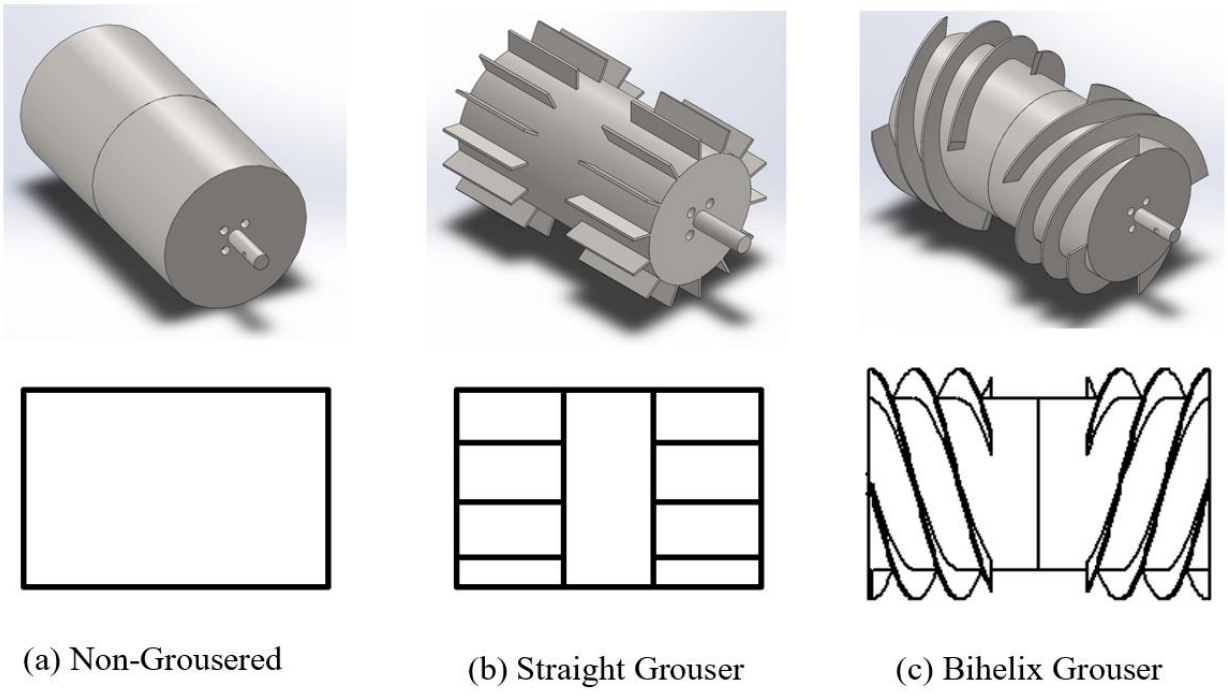

Figure 2. Grouser Wheel Designs

For this research, three main wheel geometries were investigated: non-grousered with sandpaper, straight grousered, and the bihelically-grousered. Non-grousered with sandpaper represents a typical wheel without any protrusions. The wheel soil interaction of a traditional non-grousered wheel is demonstrated in figure 3 with ω being rotational velocity, h being wheel sinkage, and Θ_f being the entrance angle. The tractive force is generated by the normal force and friction coefficient as the wheel rolls over the surface of the media [25].

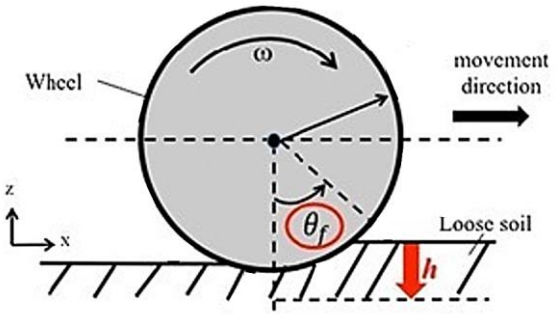

Figure 3. Non-Grousered Wheel-to-Soil Interactions

Straight grousers are the simplest grouser type, made up of parallel straight protrusions that effectively increase wheel radius. As the wheel rotates by ω, the grousers scrape the surface, picking up media and dropping it in incremental piles in the wake of the wheel. This increases the tractive load as well as the sinkage of the wheel [26].

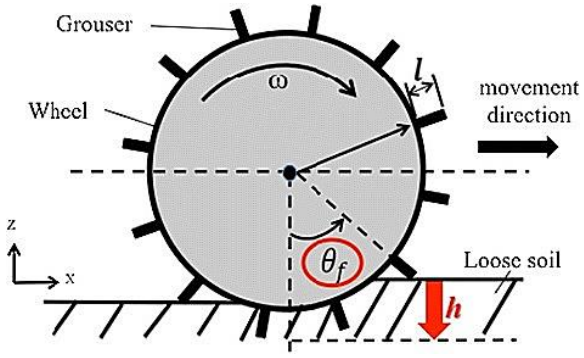

Figure 4. Straight-Grousered Wheel-to-Soil Interactions

This research investigates a novel grouser type: the bihelical-grouser. Like the V-shaped grouser, it is composed of protrusions that angle and mirror one another. However, instead of individual protrusions, each side is comprised of four equally spaced helical windings. The bihelically-grousered wheel couples rotational and translational motion, continuously displacing material to the outer perimeter of the wheel. This causes the wheel to have a larger contact surface area while not creating the obtrusive wake of

media as seen with traditional grousers. This is important for real world application since planetary vehicles typically use four or more wheels. The wheels in the front will disturb the media, leaving a wake pattern that the back wheels then need to traverse.

Figure 5. Wake Pattern of Bihelical-Grousered Wheel in BP1 (Left) and Silica Sand (Right)

In addition to grousered wheels, a major focus of this research is the use of screw propulsion to drive mobility in granular media. Understanding how the screw moves through media is helpful when designing optimal screw design through a specific environment

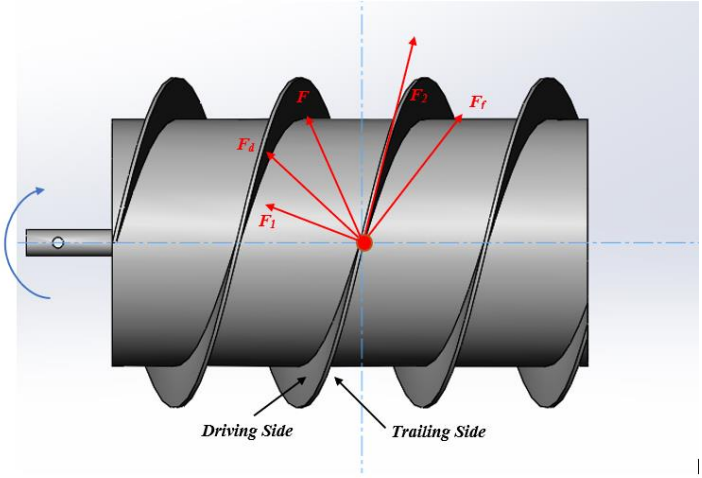

Figure 6. Forces on Archimedes Screw Geometry

As the screw rotates, the driving side of the screw blade pushes the granular media resulting in force F in newtons. F_1 and F_2 are the normal force and friction force which can be broken into the axial force and radial force. This creates the force F_d that pushes the craft forward. The trailing side also experiences a force labeled F_f [24]. The optimal angle for the pitch is 55◦ which allows for maximum forward thrust [4].

2.2 Conceptual Design

The verification of granular scaling laws requires a dynamic mobility platform that could withstand rigorous testing in granular media. In addition, GSL use input parameters such as mass and length of the intruding geometry; therefore, the mobility system had to fit different sized screws/wheels and other geometries. From these needs, the initial concept of a highly modular two wheeled mobility platform was developed.

The primary needs of the system are:

1. Be able to mount varying sized intruding geometries (both wheel and screw)
2. Have variable system mass
3. Collect translational velocity and power usage
4. System must withstand over 1000 experimental test runs in Silica Sand and BP-1

One of the main driving factors for system specifications was the size of the granular media test beds. The wheels must be able to rotate at least one full rotation while having enough room on all sides to not have any residual boundary effects caused by the

walls of the test chambers. For this research, two separate test beds were constructed to hold silica sand and BP-1. Silica sand, also known as quikrete, is not considered hazardous therefore an open aired 80 cm × 250 cm testbed was constructed using acrylic and steel brackets.

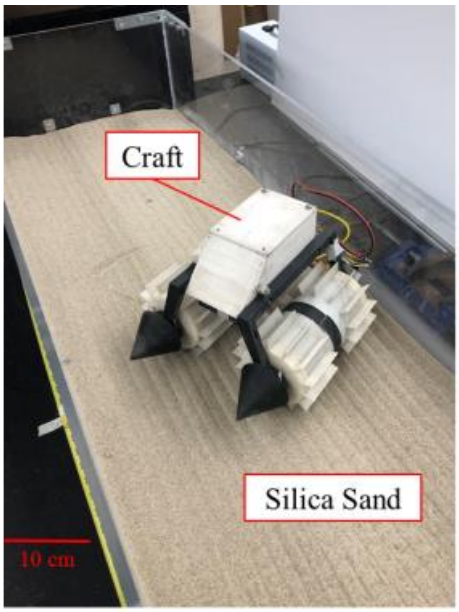

Figure 7. Silica Sand Test-Bed

Due to the particle size, extra precautions had to be made to be able to safely test in BP-1. As discussed before, 60% of particles are smaller than 110 microns and 30% are smaller than 55 microns which means the particles are small enough that, when in the air, it is a potential health hazard for humans. In order to mitigate this problem, a BP-1 chamber was custom designed and constructed so that the media was isolated from the outside world and from the researchers conducting experiments. The internal chamber is 37.5 cm × 67.5 cm, comprised of 80-20 aluminum pieces and acrylic.

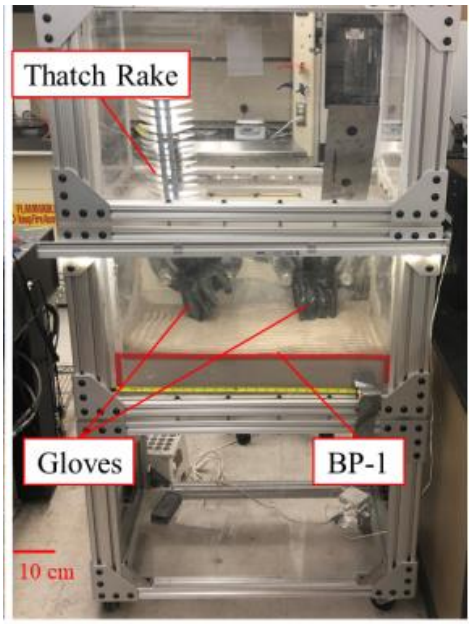

Figure 8. BP-1 Test Chamber

In order to validate GSL for wheels and screws, a total of 11 different sized screws/wheels needed to tested in BP-1 and quikrete. The goal was to minimize the time it would take to switch out wheel designs/sizes. The system had to be able to withstand over 1000 experimental test runs with minimal down time. In order to meet this requirement, it was critical for the electronics/hardware and motors to be isolated from the environment due to the negative effects that small granular particles can cause. Small particles can cause jamming, preventing the screws from rotating and causing a spike in power usage; therefore, it was determined that the screw pontoon must be designed to completely encase the motor that was driving the motion. In addition, all hardware had to be isolated from the environment in order to stop particles from getting into the electronics as the particles could conduct electricity causing system failure.

2.3 Preliminary System Design

The system was broken into 5 main subsystems to be addressed: drive-train, structure, sensing, human-system interaction, and control system [29].

The drive train had to meet size specifications restricted by size of the test chamber. For example, the largest wheel that could be tested in the BP-1 chamber had a diameter of 11.25cm which then had to be incrementally scaled down to get other sizes. A robust drive train method had to be designed to keep the motors isolated from the granular media and to ensure the intruding geometry of the wheels/screws was the only interaction with the environment.

The specifications of the structure of the system was driven primarily by the drive train and size of hardware. The structure must encase the electronics, isolating all hardware from potential harm caused by granular media environment leading to a more robust craft. The size of the body of the craft must also be able to mount the different sized wheels/screws therefore the minimum craft width was determined. In addition, the granular scaling laws scale system performance using parameters such as mass, m, and length, with the variable size wheel geometry. The mass of the overall system had to be able to be varied; therefore, an undercarriage storage system was designed so weights can be added to the system while minimizing the change in moment of inertia.

The sensing subsystem consisted of the system that collects the actual data necessary to validate the granular scaling laws. Specifically, system translational velocity and power consumption was necessary to experimentally validate the theory. For velocity, various data collection methods were evaluated such as string potentiometers,

inertial measurement units (IMUs), and cameras. Due to the size constraints of the BP-1 test chamber and accuracy in IMUs measurements, the motion capture 60 fps (frames per second) camera was selected to track the translational velocity for each run. The power used to maintain the target rpm for both the motors was calculated using the input voltage and the output current measured via current sensors. Using the following relationship, with P being power, I being current, and V being voltage, the power used for mobility was calculated.

$$P = IV \tag{1}$$

The next subsystem evaluated was the human-system interaction. This is important to consider for the overall system development lifecycle due to the quantity of experiments needed to validate these scaling laws. The human-system interaction refers to the role that humans have for maintenance of the system as well as resetting experiments. During each experiment, the mobility platform works independently to traverse the media and collect system data; however after each run the granular media in the test chambers must be reset to be as close as possible.

The granular scaling laws focus on prediction overall system behavior such as steady state velocity and power; therefore, it is important for the craft to reach steady state. The control subsystem was utilized to control rotational velocity of motors to ensure steady state is reached and maintained throughout each test run.

2.4 Detail Design and Development

The craft is comprised of the main body, housing the electronics, and two pontoons that can have the wheel or screw attachments depending on the experiments being conducted.

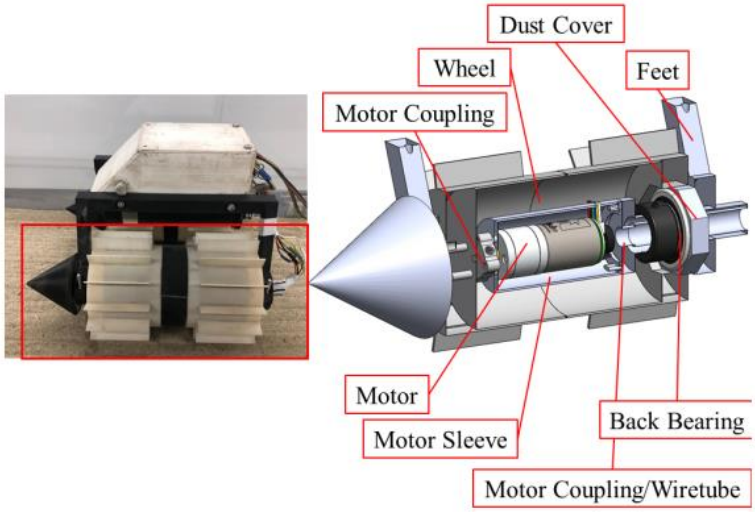

Figure 9. Inside view of Wheel with Internally Encased Motor

The electronics comprised of an Arduino, to control all hardware on the mobility system, a dual motor controller, two current sensors, and two 12V DC motors, used to drive each pontoon with an attached encoder to measure the rotational speed. The craft was tethered to a power-supply unit that was supplying a constant 12V. A proportional differentiator (PD) controller was used to control the system so that both motors rotate at a constant target rotations per minute (rpm).

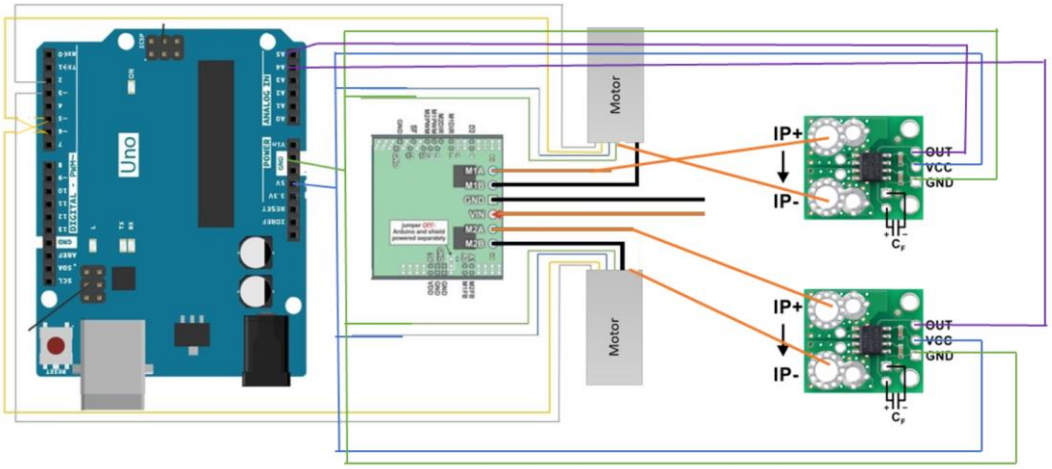

Figure 10. Wiring Schematics of Electronic Subsystem

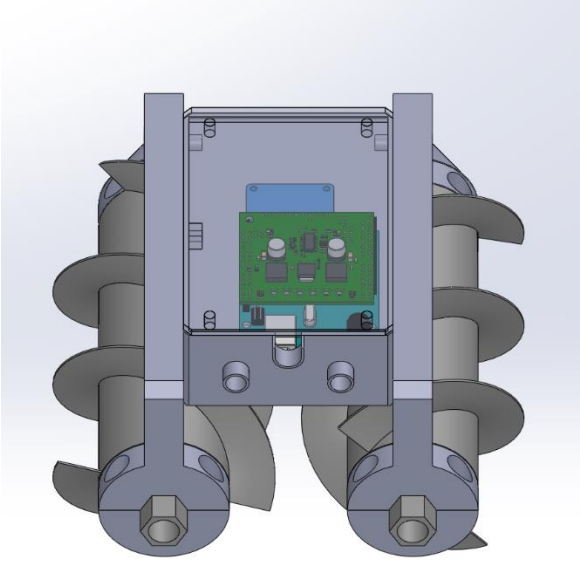

Figure 11. Electronics Mounted to Structure Model with Top Door Removed

2.5 Production and Construction

The craft is primarily composed of 3D printed Acrylonitrile Butadiene Styrene (ABS) plastic and commercial-off-the-shelf hardware. The wheel/screw geometries were printed in two main segments that allowed a smaller 3D printer test-bed size to be used. In order to get the complex geometry like a screw, a Stratasys printer was used, printing the structural parts of the craft in ABS and the supports in the polyjet support material, a dissolvable filament.

The electronics/hardware purchased included an Arduino Uno R3, two 12V 75x1 gear ratio Pololu DC motors with integrated quadrature encoders, Pololu MC33926 dual motor driver, and two Hall-effect Pololu ACS714 current sensors. The back of the screw pontoon was designed with an opening for wires to come out of which then feed back into the main body of the craft. After the wires were fed through, tape was placed over the slots, closing up potential openings for granular media to get into the craft.

After the full craft was assembled, the current usage and input rpm values were validated via benchtop testing. Quadrature encoders were attached to each motor which sends pulse signals to the Arduino as the motor rotates. These encoders use 48 pulses at a 75x1 gear ratio which ends up being 3600 counters per output shaft revolution. The Arduino counts the number of pulses and converts it to RPM. The RPM was then compared to ground truth to ensure the corresponding values reflected what was physically happening. Then the current data and voltage data was collected at different RPMs to see how much power is being used with no load on the system. These values were recorded and subtracted from future experiments.

The PD controller was implemented and Kp and Kd values were tuned so that the craft would hit the targeted rpm within a 3% error in less than 2 seconds of driving through the granular media.

Table 1. Kp and Kd Terms for PD Controller

Intruding Geometry	Kp	Kd
Straight-Grousered	0.2	0.8
Bihelical-Grousered	0.2	0.8
Helical	0.2	0.4
Non-grousered with Sandpaper	0.2	0.8

2.6 Utilization and Support

After the system is fully deployed, the utilization and support phase is used to maintain and operate the system. Resetting the testbed after each trial to start with near exact initial conditions was extremely important for maintaining valid data collection. A thatch rake was used to rake the media after each run in both horizontal and vertical directions. Then the media was leveled at the set height marked on the side of the test chamber. This effectively fluffs up the material and ensures that the porosity and compactness of the media is the same for all runs. The BP-1 chamber had to be custom built with glove holes so the user can reset the test-bed and reset the craft in the starting position while safely being isolated from the media itself.

When over a thousand experiments are conducted, it is important to stream-line the data processing. The sensor data collected for each trial was the voltage and current for each motor and the video of each trial. A motion capture 60 fps (frames per second)

camera was used to track the craft. First the camera was calibrated using a checkerboard and measuring tape to determine pixilation distance. A colored block was attached to the side of the craft then a custom color tracking program was designed to track the position of the craft over time. These values were then differentiated to get velocity over time. In order to streamline the data processing, the script would loop through the experimental videos and output distance over time and velocity over time plots. The velocity over time data was differentiated one more time to get acceleration which was used to determine steady state. At steady state, the average translational velocity and the average power were recorded and used for analysis.

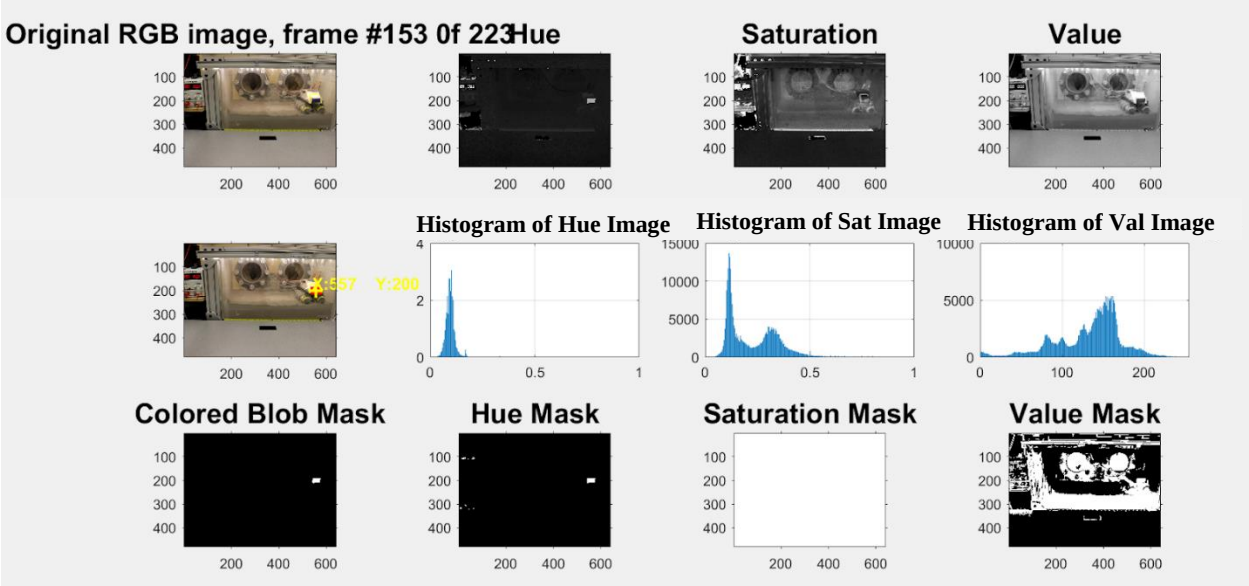

Figure 12. Color Tracking Program

CHAPTER 3

VALIDATING GRANULAR SCALING LAWS FOR WHEELS

3.1 Introduction

Granular scaling laws, or GSL, were developed for predicting system performance of arbitrarily shaped wheels in granular media. There is an unknown equation that represents the relationship between power and velocity and all the parameters that go into the wheel and environment. Despite not knowing what the equation is, the relationship between parameters can be determined using non-dimensional analysis [14, 15].

$$(P, V) = \psi(d, l, m, \omega, t, f, g, \rho, \mu, \mu_w) \quad (2)$$

The parameters that characterize the wheel are d, the diameter, l, the length, m, the mass, ω, the rotational velocity, and f the shape of wheel geometry.

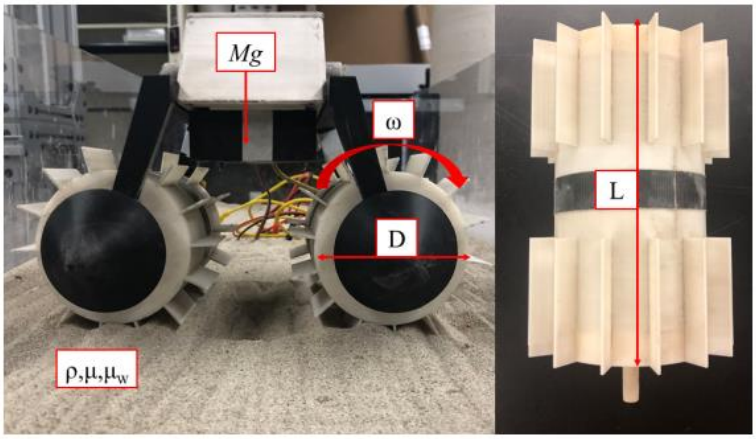

Figure 13. Wheeled System Parameters

The characteristics of the environment are g, gravity, ρ, the densiy, μ, the internal friction, and μ_w, the wheel-particle friction. The variable t is the time parameter. Using

non-dimensional analysis, each parameter was simplified into a unitless value using the base quantities of L=l, M=m, and T=1/ ω.

$$\left[\frac{P}{Mg\sqrt{Lg}}, \frac{V}{\sqrt{Lg}}\right] = \Psi\left(\frac{d}{L}, t\sqrt{\frac{g}{L}}, f, \frac{g}{L\omega^2}, \frac{\rho L^3}{M}, \mu, \mu_w\right) \quad (3)$$

Since the characteristics of the environment are all held constant, the main parameters focused on are the scaling of the craft itself which can be simplified to the following equation:

$$\left[\frac{P}{Mg\sqrt{Lg}}, \frac{V}{\sqrt{Lg}}\right] = \widetilde{\Psi}\left(\frac{1}{L\omega^2}, \frac{dL^2}{M}\right) \quad (4)$$

Using the equation above, the scalars r and s demonstrate the scalar relationship for the dimensions of the wheel geometry

$$(l', m', d', \omega') = \left(rl, sm, \frac{s}{r^2}d, \frac{1}{\sqrt{r}}\omega\right) \quad (5)$$

The time-averaged power and translational steady state velocity are found using the same s and r scalars using the following relationships:

$$P' = s\sqrt{r}P \quad (6)$$

$$V' = \sqrt{r}V \quad (7)$$

These scaling laws were derived and validated via simulations and experiments [,]. They were tested on a wheel on a gantry in silica sand, measuring velocity and power. The wheels tested were non-grousered wheels with sandpaper and a lug wheel design; however they were not experimentally tested on a dynamic mobility system. Due to the nature of granular media, there is high variability in environment based on factors such as

compactness. Most vehicles, both planetary and Earthwise, utilize four wheels with the back wheels behind the front wheels. This causes the back wheels to have to drive over media that has already been disturbed by the front wheels, which was not researched in initial GSL validation. By having two wheels on the dynamic mobility platform, the granular scaling laws can be validated in conditions that are more realistic to what a vehicle will actually experience.

3.2 Method

Validation of GSL was performed using the dynamic mobility platform with two wheels mounted side by side on craft so that trailing wheel drives through the media that the previous wheel had disturbed. As a base experiment, non-grousered wheels with sandpaper were tested in Quikrete. This experiment was conducted as a comparison to the experiments that validated GSL at MIT Robotic Mobility Group Lab. This lab conducted experiments of a single non-grousered wheel with sandpaper in Quikrete, the same type of silica sand utilized in our experiments, on a gantry system [15]. In this research, two different sized sandpaper wheels were tested. Then straight-grousered wheels were tested. The notation SP in GSL1SP stands for Sand Paper while the G stands for Grousered. The 1 in GSL1SP represents the smaller size while 2 represents the larger size.

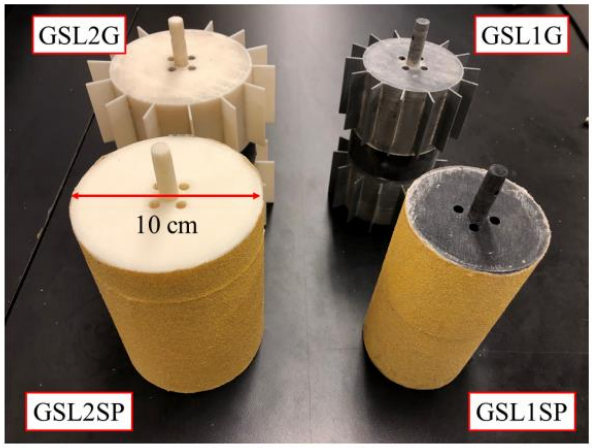

Figure 14. Two sizes of Wheel, Non-Grousered and Straight-Grousered

In these trials, different scaled masses and lengths for wheels were tested to validate the effective predictive capabilities of GSL. Using the scaling equation:

$$(l', m', d', \omega') = \left(rl, sm, \frac{s}{r^2} d, \frac{1}{\sqrt{r}} \omega\right) \quad (5)$$

The length and mass would be scaled by scalars r and s. Then these scalars are used to find out how much the diameter and rotational velocity should change. Using these relationships, the following test properties for sandpaper and straight-grousered wheels were found.

Table 2. Sandpaper and Straight Grousered Wheel Properties

Name	Diameter	Masses	Depth	Grouser	RPM
GSL1G	7.5	1.46, 2.19, 2.92	14	1.25	15,30,45,60,75
GSL2G	10	2.59, 3.84, 5.19	14	1.667	13,26,39,52,65
GSL1SP	7.5	1.46, 2.92	14	N/A	15,30,45,60,75
GSL2SP	10	2.59, 5.19	14	N/A	13,26,39,52,65

For these experiments, two different sizes for straight-grousered wheel and sandpaper wheels were tested at various different masses. The masses were varied by

adding weights to the undercarriage of the craft. Five different rotational velocities were tested using the scaled $\frac{1}{\sqrt{r}}\omega$ to get the new rotational velocities for the new sized craft.

The same process was done for 3 different sizes for both straight-grousered wheels and bihelical-grousered wheels in the quikrete as well as the BP-1; however only one mass is tested for each wheel geometry.

Figure 15. Bihelix-Grousered Wheels and Straight-Grousered Wheels

The notation for the wheels are GSL followed by a number indicating the relative size of the wheel and the letter notating the type of grouser, G for grousered and B for bihelix. GSL1B describes the smallest size bihelical grousered wheel whereas GSL3G represents the largest straight grousered wheel. The same scaling relationship completed using the relationships in equation 5. For these experiments, the mass was held constant for each scale of geometry. The goal was to

Table 3. Straight-Grousered and Bihelix-Grousered Wheel Properties

Name	Diameter	Masses	Depth	Grouser	RPM
GSL1G	7.5	1.46	14	1.25	15,30,45,60,75

GSL2G	11.25	2.59	14	1.875	13,26,39,52,65
GSL3-G	9.375	2.918	18	1.5625	14,27,40,54,67
GSL1-B	7.5	1.477	14	1.25	15,30,45,60,75
GSL2-B	11.25	2.626	14	1.875	13,26,39,52,65
GSL3-B	9.375	2.954	18	1.5625	14,27,40,54,67

Twelve trials were conducted at five different rotational speeds for each size and mass in silica sand and BP-1. A total of 920 experimental runs were conducted, with the primary measured data being the translational velocity and power. Each trial comprised of setting the craft on a reset test-bed and specifying the rotational velocity. The craft would traverse over the sand/BP-1 while velocity and power data was collected via the 60 fps motion capture camera with color tracking software and on board current sensors for each motor. The craft would reach near the end of the testbed and the power supply would be cut off to stop the craft. The testbed would be reset and the trials would occur all over again.

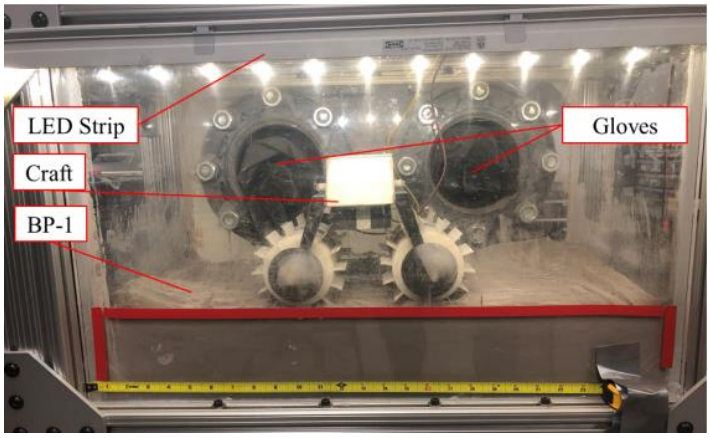

Figure 16. View of Inside BP-1 Chamber with Straight-Grousered Wheels Mounted to Craft

3.3 Results

After analyzing the non-grousered sandpaper wheels and straight grousered wheels with variable masses in quikrete, it is apparent that there is a mass dependency with the predictive capability of GSL. The sandpaper wheel experiment should have been directly comparable to the single wheel sandpaper experiment that was conducted in literature; however high errors were seen in the power predictions.

Table 4. Power Ratios and Errors for Mass-Dependent Predictions

Name	RPM	Power Ratio	Percent Error
GSLSP Light	13	1.59	22.6%
	26	1.47	28.1%
	39	1.38	32.8%
	52	1.55	24.2%
	65	1.48	27.3%
GSLSP Heavy	13	1.59	3.6%
	26	1.47	9.1%
	39	1.38	10.9%
	52	1.55	14.5%
	65	1.48	17.3%
GSLG Light	13	1.48	27.7%
	26	1.64	20.1%
	39	1.59	22.4%
	52	1.54	25.0%
	65	1.49	22.3%
GSLG Medium	13	1.70	17.2%
	26	1.66	19.0%
	39	1.70	17.1%
	52	1.65	19.5%
	65	1.66	18.6%
GSLG Heavy	26	1.84	10.3%
	39	1.80	12.4%
	52	1.77	13.5%

At the lighter weights, errors for power ratio ranged from 23% to 33%. This error is extremely high. It was interesting that the higher error occurred at the middle rotational velocity. Normally higher discrepancies in data occurs at the more extreme ranges such as the lowest RPM or highest RPM. At the heavier loads, this error is drastically reduced with errors ranging from 4% to 17%. Similar trends occurred for the straight grousers however the percent error did not range as much as the sandpaper wheels. The error for the light tests ranged from 20% to 28%. The straight grousers were also tested at a medium weight, with percent error ranging from 17% to 20% and at heavy weight, with percent error ranging from 10% to 14%. As the mass increased, the error percentage reduced. This demonstrates there is a clear mass dependency on the GSL. This is likely due to lack of full engagement of the intruding geometry which causes the system to slip. As slip begins to increase, the scaling laws lose accuracy in effective predictability. This is something that will have to be incorporated into design decisions, especially for space application since gravity is lesser and the weight for a given mass would be even lower.

The next set of experiments analyzed were the different sized straight and bihelix grousered wheels. These wheels were tested in both BP-1 and Quikrete therefore two plots were created for power comparisons and velocity comparisons.

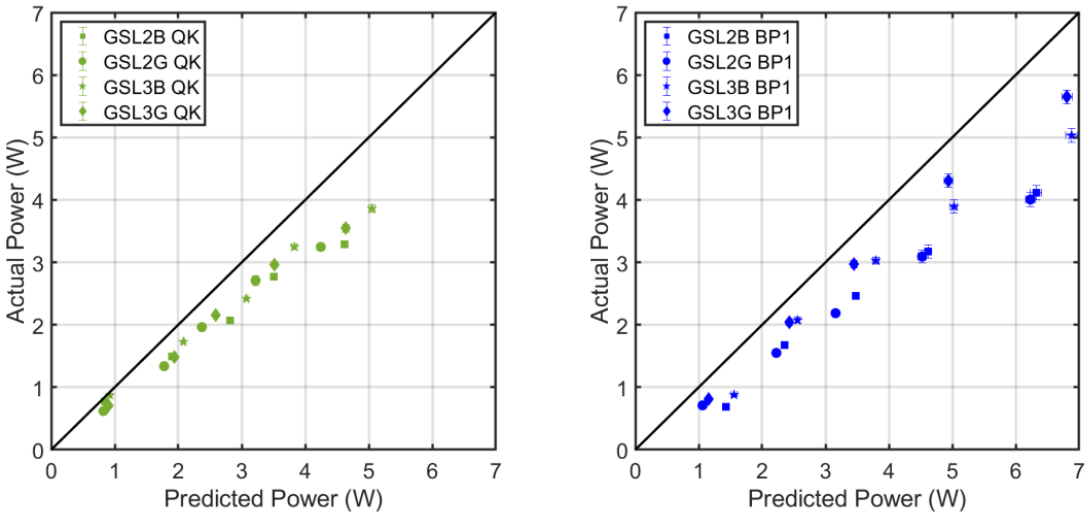

Figure 17. Actual Power Vs Predicted Power

For both Quikrete and BP-1, the actual power was less than the predicted power. According to figure 21, as rotational velocity increases the difference between the actual power and predicted power increases meaning the percent error increases at higher RPMs.

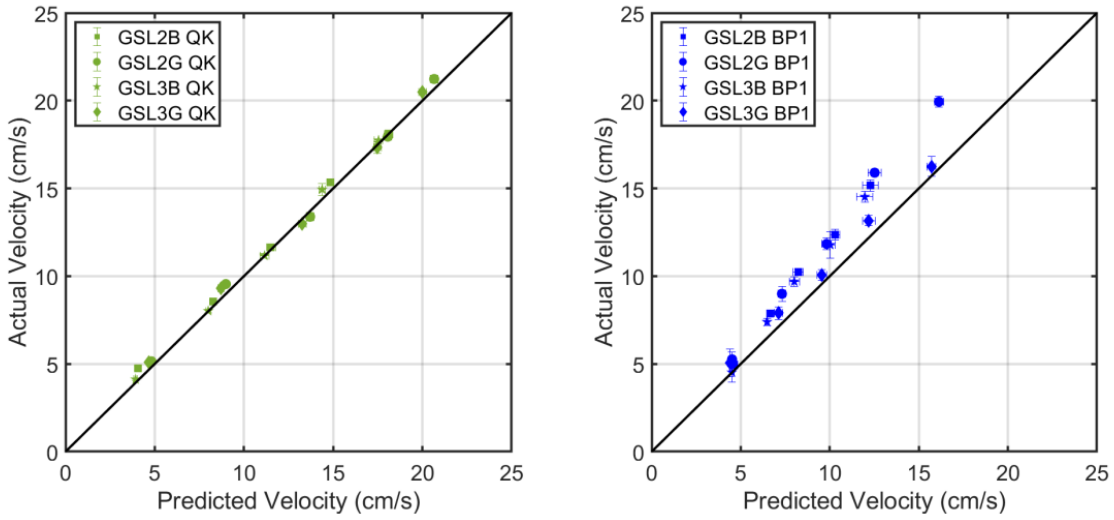

Figure 18. Actual Translational Velocity Vs Predicted Velocity

The actual velocity vs predicted velocity, demonstrated fairly accurate velocity estimates in Quikrete. The GSL underpredicted the actual velocity in BP-1. This means the craft ended up going faster than what was predicted using GSL despite using less actual power than predicted. This percent error also increased as rpm increased. This could be due to a variety of different reasons, one of which could be that the original lower sized wheel experiments in which the predictions were based off of could have pulled more power and gone slower due to slippage. The lowest sized wheels had the lowest mass which as seen in prior experiments, low mass in a light-weight system is correlated to higher errors.

CHAPTER 4

VALIDATING HELICAL GRANULAR SCALING LAWS

4.1 Introduction

The granular scaling laws for arbitrarily shaped wheels were then applied to helical geometries. Using non-dimensional analysis, a set of relationships were derived relating the mass and length which is related to the pitch. Initial assumptions for these laws to be valid is that helical shape is radially constant and the screw radii and blade radii are constant.

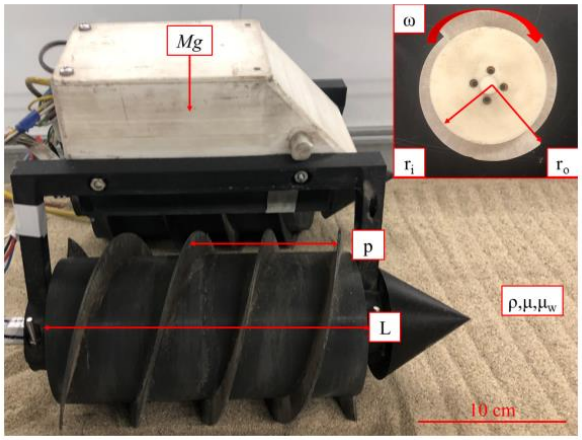

Figure 19. Parameters of Craft and Screw Geometry

The initial relationship for power, P, and translational velocity, V, is

$$(P, V) = \psi(p, r_i, r_o, l, m, \omega, t, f, g, \rho, \mu, \mu_s) \quad (8)$$

where p is the pitch, r_i is inner radius, r_o is outer radius, l is length, m is mass, ω is rotational velocity, ρ is density, μ is internal friction, μ_s is screw-grain friction, g is gravity, and t is time. The parameter f is the function that describes the screw geometry profile [27,28]. The actual equation, ψ, is unknown; however we know there is a

relationship between these geometry parameters and these environmental parameters that end up resulting in power and translational velocity. Non-dimensional analysis was conducted on these parameters and the following relationship was found:

$$\left[\frac{P}{Mg\sqrt{Lg}}, \frac{V}{\sqrt{Lg}}\right] = \Psi\left(\frac{r_i}{p}, \frac{r_o}{p}, \frac{l}{p}, t\sqrt{\frac{g}{p}}, f, \frac{g}{p\omega^2}, \frac{\rho p^3}{M}, \mu, \mu_s\right) \quad (9)$$

Then with constant gravity and looking at steady state.

$$\left[\frac{P}{M\sqrt{p}}, \frac{V}{\sqrt{p}}\right] = \widetilde{\Psi}\left(\frac{r_i}{p}, \frac{r_o}{p}, \frac{lp^2}{M}, \frac{1}{p\omega^2}, \frac{1}{\sqrt{p}}t\right) \quad (10)$$

Using the above relationship, scaled power predictions and scaled velocity predictions were found:

$$(p', l', m', r_i', r_o', \omega') = \left(ap, ba^{-2}l, bM, ar_i, ar_o, \frac{1}{\sqrt{a}}\omega\right) \quad (11)$$

Positive scalars a and b were obtained from the above relationship and then used to predict power and velocity at steady state.

$$P' = b\sqrt{a}P \quad (12)$$

$$V' = \sqrt{a}V \quad (13)$$

4.2 Method

Two screws were mounted on the mobility platform side by side so that both screws would touch undisturbed media as it travels through the granular media. Like in previous experiments, three sizes were tests, notated by HGSL for Helical Granular Scaling Law and then a numeric to label which size it is with 1 being the smallest and 3 being the largest.

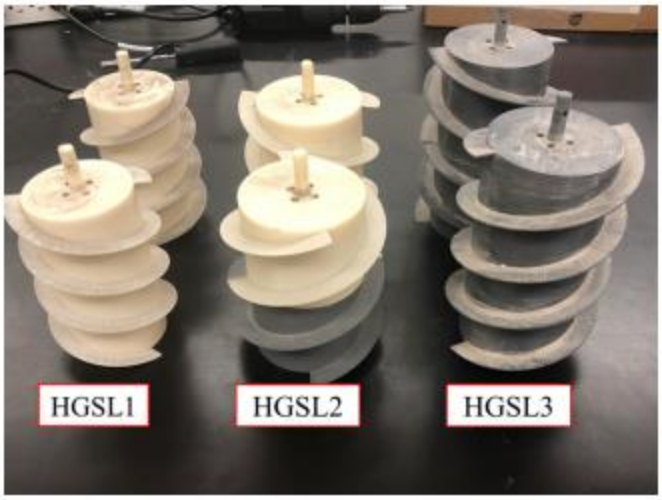

Figure 20. Three sizes of screw geometry

First, HGSL1 was tested at five different rpms in BP-1. The test procedure followed similar trend to the wheel experiments except for the screws are side by side and counter-rotating. By churning outwards, the screws propel the system forward while piling excess media on the outskirts of the path.

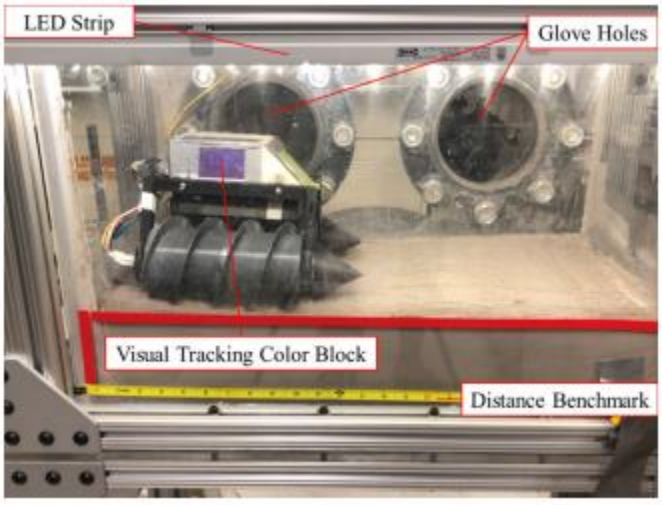

Figure 21. View of Inside of BP-1 Chamber the Screw Pontoons Mounted in Starting Position for an Experimental Trial

The velocity and power data was then used to find the scaling law parameters for the scaled up version with scalars a and b.

$$(p', l', m', r_i', r_o', \omega') = \left(ap, ba^{-2}l, bM, ar_i, ar_o, \frac{1}{\sqrt{a}}\omega\right) \quad (11)$$

Below is a table of all of the parameters for the helical pontoons that were tested.

Table 5. Helical Pontoon Properties

Name	Pitch	Mass	Depth	r_i	r_o	RPM
HGSL1	7.5	1.441	14	3.75	5	15, 30, 45, 60, 75
HGS2	9	2.075	14	4.5	6	13.7, 27.4, 41.0, 54.8,68.5
HGSL3	9	2.666	18	4.5	6	13.7, 27.4, 41.0, 54.8,68.5

4.2 Results

The smallest size of helices, HGSL1, was tested in BP-1 and used predict the power and velocities for HGSL2 and HGSL3. These predicted values were then compared to the actual values obtained through experimental testing. The results demonstrated a power prediction error of 3-9% and velocity prediction error of 2-12%, which is actually better than the wheel experiments. The larger size, HGSL3, demonstrated a slightly higher power draw than predicted; however HSL2 followed the prediction line very closely. For velocity, HGSL2 actual velocity was higher than the predicted values.

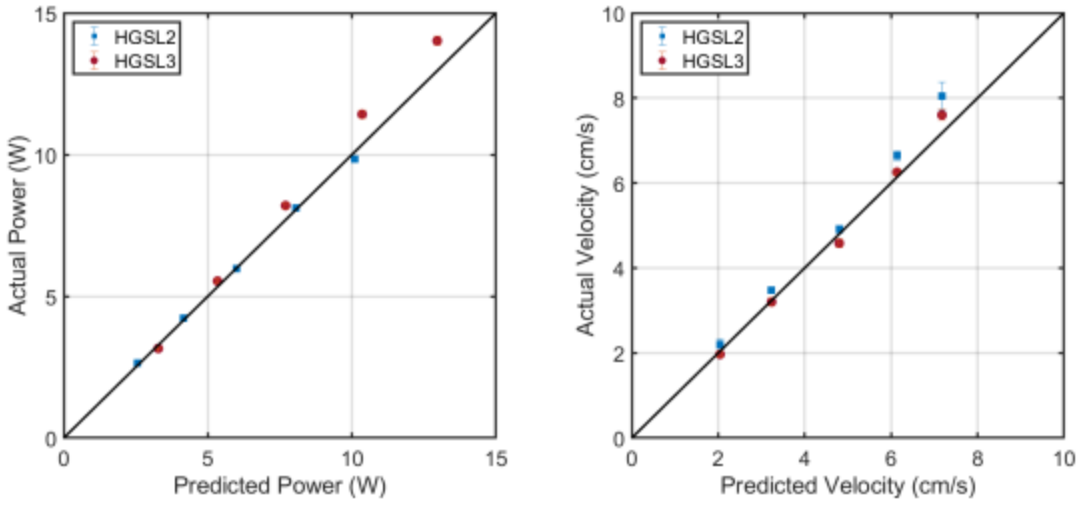

Figure 22. Actual Power Vs Predicted Power Results for Helical Granular Scaling Laws (Left) and Actual Translational Velocity Vs Predicted Velocity (Right) in BP-1

The main hypothesis behind the wheel granular scaling laws' inaccuracies is due to the intruding geometry not fully engaging with the media due to the light-weight nature of the craft. Screw geometries however do not just roll on the surface, but actually dig through the media, propelling the craft forward. The helical blades have increased contact area with the media compared to its wheel counterpart and displaces the media to the outside of the craft as it drives. The geometry of the screw naturally will engage more fully with the media so it makes sense that the helical scaling laws are more accurate in light-weight systems than its wheel alternative.

CHAPTER 5

CONCLUSIONS AND FUTURE WORK

5.1 Conclusions

Granular scaling laws can be an effective tool for predicting scaled system performance through granular media. This can drastically reduce cost of prototyping as you can test the system at a smaller scale; however, the scaling laws are not applicable for every situation. GSL for light-weight mobility systems has a drop off in effectiveness as the mass of the system decreases. This is caused by the lack of full engagement of the intruding geometry with the granular media. Unlike wheels, screw propelled mobility systems move through the granular media, not just on top, therefore the helical geometry remains in full contact with the media. The recently developed helical scaling laws demonstrate valuable predictive capabilities despite being applied to a light-weight systems. This is especially important for space application as light-weight systems are significantly less expensive to get into earth orbit and beyond. In addition, effectiveness of wheels is dependent on getting enough traction, which is not always possible in low gravity environments. Wheels need to fully engage with the environment in order to effectively move and minimize slippage; however, screw propulsion represents a potential alternative mobility method.

5.2 Future Work

This research on granular scaling laws has many possible interesting research avenues that can be taken. BP-1 is an interesting material to study as it has high research interest within the space community as well as the granular physics community. Due to

the angularity of BP-1 particles, the high inter-particle frictional force causes an almost cohesive-like effect; however, the helical granular scaling law's predictive capabilities were still fairly accurate. For future work, the granular scaling laws will be investigated in cohesive media for both wheel and screw intruder geometries. An initial derivation of GSL for cohesive media was completed; however, the verification and validation of this model must still be done.

5.2.1 Scaling Laws for Cohesive Granular Media

Various types of granular media can have a cohesive effect that vastly alters the behavior of the media. For example, the silica sand can easily be altered into a cohesive media by adding hydration. The sand then becomes mud and the interaction between the media and the screw/wheel becomes vastly different. One media that has high interest within the space community is ice. Sensor data has revealed that extraterrestrial bodies like Enceladus and Europa have ice on the surface as well as ice crevasses that can be explored deep into the surface. The surface of Enceladus is believed to be sintered ice, which is ice that has been broken up into particles [19]. This environment can be modeled as a type of granular media that has a high cohesion.

Several models for ice were investigated such as cohesive zone modelling [31], Coulomb's law [32], and cohesive force of ice particles in ice slurry [33]. The Kelvin-Voigt model was ultimately chosen due to its applicability in modelling the brittle nature of ice at the desired temperatures and loading rates. This model treats ice as a viscoelastic material, using a spring and damper in parallel to model the internal stress between ice particles [30].

The following equation demonstrates the Kelvin-Voigt model, with σ being stress, E the elastic modulus, η the viscosity, and ε the strain [30, 34].

$$\sigma = E\varepsilon + \eta\dot{\varepsilon} \tag{14}$$

The key inputs for the power and velocity equation include both screw design and environmental factors. The screw design inputs include factors such as pitch (p), inner radius (r_i), outer radius (r_o), length (l), mass (m) and rotational velocity (ω). Key inputs based on the environment are ice density (ρ), screw-ice friction (μ_s), gravity (g), time (t), and stress (σ). Note that the stress term σ represents the Kelvin-Voigt model mentioned above and encompasses the cohesion and friction relationship between particles.

$$[P, V] = f(r_i, r_o, l, m, \omega, \rho, \mu_s, g, t, E, \varepsilon, \eta, \dot{\varepsilon}) \tag{15}$$

Table 6. Locomotion Parameters and Dimensionless Expressions

Parameter	Dimension	Dimensionless Parameter	Variable Expression
$[P]$	$[\frac{ML^2}{T^3}]$	$\underline{P}$	$[\frac{P}{mg\sqrt{pg}}]$
$[V]$	$[\frac{L}{T}]$	$\underline{V}$	$[\frac{V}{\sqrt{pg}}]$
$[p]$	$[L]$	$\underline{p}$	1
$[r_i]$	$[L]$	$\underline{r_i}$	$[\frac{r_i}{p}]$
$[r_o]$	$[L]$	$\underline{r_o}$	$[\frac{r_o}{p}]$

[l]	[L]	$\underline{L}$	$[\frac{l}{p}]$
[m]	[M]	$\underline{m}$	1
[ω]	$[\frac{1}{T}]$	$\underline{\omega}$	1
[ρ]	$[\frac{L^3}{M}]$	$\underline{\rho}$	$[\frac{\rho p^3}{m}]$
$[\mu_s]$	[none]	$\underline{\mu_s}$	$[\mu_s]$
[g]	$[\frac{L}{T^2}]$	$\underline{g}$	$[\frac{g}{p\omega^2}]$
[t]	[T]	$\underline{t}$	$[t\sqrt{\frac{g}{p}}]$
[E]	$[\frac{M}{T^2L}]$	$\underline{E}$	$[\frac{E}{\rho g p}]$
[ε]	[none]	$\underline{\varepsilon}$	[ε]
[η]	$[\frac{M}{TL}]$	$\underline{\eta}$	$[\frac{\eta p}{\omega m}]$
[ὲ]	$[\frac{1}{T}]$	$\underline{\grave{\varepsilon}}$	$[\frac{\grave{\varepsilon}}{\omega}]$

First the function must be transformed using non-dimensional analysis. The base quantities used to cancel out the base quantities for each parameter are length (L), mass (M), and time (T).

$$L = p, \qquad M = m, \qquad T = \frac{1}{\omega} = \sqrt{\frac{p}{g}} \qquad (16), (17), (18)$$

An example of the procedure is given for gravity.

$$\underline{g} = g\frac{T^2}{\omega} = \frac{g}{l\omega^2} \tag{19}$$

This procedure was conducted for all the parameters.

$$\left[\frac{P}{mg\sqrt{pg}}, \frac{V}{\sqrt{pg}}\right] = \psi\left(\frac{r_i}{p}, \frac{r_o}{p}, \frac{l}{p}, \frac{m}{m}, \frac{\omega}{\omega}, \frac{\rho p^3}{m}, \mu_s, \frac{g}{p\omega^2}, t\sqrt{\frac{g}{p}}, \frac{E}{\rho g p}, \varepsilon, \frac{\eta p}{\omega m}, \frac{\dot{\varepsilon}}{\omega}\right) \tag{20}$$

Several assumptions were made to simplify the above equation.

1. The ice is homogenous between experiments therefore density and screw-ice friction are assumed to be constant between experiments.
2. Gravity is constant between experiments; therefore gravity was also eliminated as a functional variable.
3. Screw shape f is constant
4. Engineers mostly concerned with overall characteristics of screw design and therefore only look at steady-state performance of craft; therefore time (t) has been eliminated entirely as a dimensionless parameter

$$\left[\frac{P}{m\sqrt{p}}, \frac{V}{\sqrt{p}}\right] = \psi\left(\frac{r_i}{p}, \frac{r_o}{p}, \frac{l}{p}, \frac{p^3}{m}, \frac{1}{p\omega^2}, \frac{E}{p}, \varepsilon, \frac{\eta p}{\omega m}, \frac{\dot{\varepsilon}}{\omega}\right) \tag{21}$$

The two independent variables are c and h. The detailed non-dimensional analysis process for each parameter can be found in Appendix A. The final equivalent relationships can be expressed in terms of the original variables and 2 scalars.

$$l' = cl,\ r_i' = cr_i,\ r_o' = cr_o,\ p' = cp,\ \omega' = h\omega,\ m' = c^3m,\ E' = cE,\ \eta' = c^2h\eta,\ \dot{\varepsilon}' = h\dot{\varepsilon} \tag{22}$$

$$P' = h\sqrt{c}P,\ V' = \sqrt{c}V \qquad (23), (24)$$

The next steps would be to validate these scaling laws by conducting experiments either physically and/or via simulations.

REFERENCES

[1] Eltawahni, H. A., & Yu, A. B. (2019, April 29). *Powder Processing: Models and simulations*. Reference Module in Materials Science and Materials Engineering. Retrieved March 31, 2022, from https://www.sciencedirect.com/science/article/pii/B9780128035818116510

[2] LU, K. E. V. I. N., BRODSKY, E. E., & KAVEHPOUR, H. P. (2007). Shear-weakening of the transitional regime for granular flow. Journal of Fluid Mechanics, 587, 347–372. https://doi.org/10.1017/s0022112007007331

[3] Stoeser, D. B., Rickman, D. L., & Wilson, S. (2010). Preliminary geological findings on the BP-1 simulant.

[4] Thoesen, A., McBryan, T., Mick, D., Green, M., Martia, J., & Marvi, H. (2020). Granular scaling laws for helically driven dynamics. Physical Review E, 102(3). https://doi.org/10.1103/physreve.102.032902

[5] Suescun-Florez, E., Roslyakov, S., Iskander, M., & Baamer, M. (2015). Geotechnical properties of BP-1 lunar regolith simulant. Journal of Aerospace Engineering, 28(5), 04014124. https://doi.org/10.1061/(asce)as.1943-5525.0000462

[6] V. Nardelli et al. 'An experimental investigation of the micromechanics of Eglin sand'. In: Powder Technology 312 (2017), pp. 166–174. doi: https://doi.org/10.1016/j.powtec.2017.02.009. url: https://www.sciencedirect.com/science/article/pii/S0032591017301262

[7] Huiyang Luo et al. 'Effect of mass density on the compressive behavior of dry sand under confinement at high strain rates'. In: Experimental mechanics 51.9 (2011), pp. 1499–1510.

[8] 'Commercial Grade Sands: Material Data Safety Sheet'. In: Quikrete Cement and Concrete Products. 2010.

[9] Zhang, T., & Goldman, D. I. (2014). The effectiveness of resistive force theory in granular locomotion. Physics of Fluids, 26(10), 101308. https://doi.org/10.1063/1.4898629

[10] Ryan D Maladen et al. "Undulatory swimming in sand: subsurface locomotion of the sandfish lizard". In: science 325.5938 (2009), pp. 314–318.

[11] Yang Ding, Nick Gravish, and Daniel I Goldman. “Drag induced lift in granular media”. In: Physical Review Letters 106.2 (2011), p. 028001.

[12] Sachith Dunatunga and Ken Kamrin. “Continuum modelling and simulation of granular flows through their many phases”. In: Journal of Fluid Mechanics 779 (2015), pp. 483–513.

[13] Ross L Hatton et al. “Geometric visualization of self-propulsion in a complex medium”. In: Physical review letters 110.7 (2013), p. 078101.

[14] Townsend, S. (S. C. (1970, January 1). Deriving and verifying a general granular locomotion scaling law. Retrieved March 30, 2022, from https://dspace.mit.edu/handle/1721.1/119936

[15] Slonaker, J., Motley, D. C., Zhang, Q., Townsend, S., Senatore, C., Iagnemma, K., & Kamrin, K. (2017). General scaling relations for locomotion in Granular Media. Physical Review E, 95(5). https://doi.org/10.1103/physreve.95.052901

[16] Jensen, R. P., Bosscher, P. J., Plesha, M. E., & Edil, T. B. (1999). DEM simulation of granular media—structure interface: Effects of surface roughness and particle shape. *International Journal for Numerical and Analytical Methods in Geomechanics*, *23*(6), 531–547. https://doi.org/10.1002/(sici)1096-9853(199905)23:6<531::aid-nag980>3.0.co;2-v

[17] Guo, N., & Zhao, J. (2014). A coupled FEM/DEM approach for hierarchical multiscale modelling of Granular Media. *International Journal for Numerical Methods in Engineering*, *99*(11), 789–818. https://doi.org/10.1002/nme.4702

[18] Thoesen, A., Ramirez, S., & Marvi, H. (2019). Screw-generated forces in Granular Media: Experimental, computational, and analytical comparison. *AIChE Journal*, *65*(3), 894–903. https://doi.org/10.1002/aic.16517

19] Dhaouadi, W., Marteau, E., Kolvenbach, H., Choukroun, M., Molaro, J. L., Hodyss, R., & Schulson, E. M. (2021). Discrete element modeling of planetary ice analogs: Mechanical behavior upon sintering. *Granular Matter*, *24*(1). https://doi.org/10.1007/s10035-021-01167-6

[20] MJ Neumeyer and BD Jones. “The marsh screw amphibian”. In: Journal of Terramechanics 2.4 (1965), pp. 83–88.

[21] Ken Evans. “The history, challenges, and new developments in the management and use of bauxite residue”. In: Journal of Sustainable Metallurgy 2.4 (2016), pp. 316–331.

[22] Liang Ju et al. “Experimental results of a novel amphibian solution for aquatic robot”. In: Robotics and Automation (ICRA), 2010 IEEE International Conference on. IEEE. 2010, pp. 2261–2266.

[23] *HMS Engineering*. HMS Engineering (Hereford) Ltd. (n.d.). Retrieved March 30, 2022, from http://www.hmsengineering.co.uk/sbird.html

[24] Nagaoka, K., Sawada, K., & Yoshida, K. (2019, August 24). *Shape effects of wheel grousers on traction performance on Sandy Terrain*. Journal of Terramechanics. Retrieved April 5, 2022, from https://www.sciencedirect.com/science/article/pii/S0022489819301041

[25] Qi, H., & You, B. (n.d.). *Control strategy for the pseudo-driven wheels of multi-wheeled mobile robots based on dissociation by degrees-of-freedom*. IEEE Xplore. Retrieved April 5, 2022, from https://ieeexplore.ieee.org/document/9177032

[26] Iizuka, K., Sasaki, T., Suzuki, S., Kawamura, T., & Kubota, T. (2014, October 21). *Study on grouser mechanism to directly detect sinkage of wheel during traversing loose soil for lunar exploration Rovers - ROBOMECH Journal*. SpringerOpen. Retrieved April 5, 2022, from https://robomechjournal.springeropen.com/articles/10.1186/s40648-014-0015-6

[27] Gong, J., Fu, Y.-F., Xia, W., Li, J.-H., & Zhang, F. (2016). Fatigue life prediction of screw blade in screw sand washing machine under random load with Gauss Distribution. American Journal of Engineering and Applied Sciences, 9(4), 1198–1212. https://doi.org/10.3844/ajeassp.2016.1198.1212 b.i

[28] Thoesen, A., McBryan, T., & Marvi, H. (2019). Helically-driven granular mobility and gravity-variant scaling relations. RSC Advances, 9(22), 12572–12579. https://doi.org/10.1039/c9ra00399a

[29] What are the three major parts and six subsystems of the industrial robot system? Shenzhen Reeman Intelligent Equipment Co., Ltd. (n.d.). Retrieved March 30, 2022, from https://www.reemanrobot.com/info/what-are-the-three-major-parts-and-six-subsyst-64178032.html

[30] Lilja, V.-P., Polojärvi, A., Tuhkuri, J., & Paavilainen, J. (2019, September 9). *Effective material properties of a finite element-discrete element model of an ice sheet*. Computers & Structures. Retrieved March 31, 2022, from https://www.sciencedirect.com/science/article/pii/S0045794918316328

[31] Zarasvand, K. A., Mohseni, M., & Golovin, K. (2021, January 4). *Cohesive zone analysis of cylindrical ice adhesion: Determining whether interfacial toughness or strength controls fracture*. Cold Regions Science and Technology. Retrieved March 31, 2022, from https://www.sciencedirect.com/science/article/pii/S0165232X20304663#!

[32] Gribanov, I., Taylor, R., & Sarracino, R. (2018, April 26). Cohesive zone micromechanical model for compressive and tensile failure of polycrystalline ice. *Engineering Fracture Mechanics*. https://www.sciencedirect.com/science/article/pii/S0013794417310561.

[33] Bassis, J. N., & Walker, C. C. (2011). Upper and lower limits on the stability of calving glaciers from the yield strength envelope of ice. *Proceedings of the Royal Society A: Mathematical, Physical and Engineering Sciences*, *468*(2140), 913–931. https://doi.org/10.1098/rspa.2011.0422

[34] Matsumoto, K., Kubota, H., Umehara, Y., Ehara, K., Sakamoto, J., Ueda, J., & Sato, K. (2018, April 4). Investigation on cohesive force of ice particles in ice slurry for long-term ice storage. *International Journal of Refrigeration*. https://www.sciencedirect.com/science/article/pii/S0140700718301063.

APPENDIX A

COHESIVE GSL NON-DIMENSIONAL ANALYSIS

Non-dimensional analysis of all parameters for cohesive granular scaling laws:

$$r_i' = ar_i, \qquad r_o' = br_o, \qquad p' = cp, \qquad l' = dl, \qquad m' = fm, \qquad \omega' = h\omega,$$

$$E' = jE, \qquad \varepsilon' = k\varepsilon, \qquad \eta' = n\eta, \qquad \dot{\varepsilon}' = q\dot{\varepsilon}, \qquad P' = sP, \qquad V' = vV$$

$$\underline{\psi}_1 = \frac{r_i}{p} \rightarrow {\psi_1}' = \frac{ar_i}{cp} \qquad \underline{\psi}_1 = {\psi_1}' \rightarrow \frac{r_i}{p} = \frac{ar_i}{cp} \qquad a = c$$

$$\underline{\psi}_2 = \frac{r_o}{p} \rightarrow {\psi_2}' = \frac{br_o}{cp} \qquad \underline{\psi}_2 = {\psi_2}' \rightarrow \frac{r_o}{p} = \frac{br_o}{cp} \qquad b = c$$

$$\underline{\psi}_3 = \frac{l}{p} \rightarrow {\psi_3}' = \frac{dl}{cp} \qquad \underline{\psi}_3 = {\psi_3}' \rightarrow \frac{l}{p} = \frac{dl}{ap} \qquad d = c$$

$$\underline{\psi}_4 = \frac{p^3}{m} \rightarrow {\psi_4}' = \frac{c^3p^3}{fm} \qquad \underline{\psi}_4 = {\psi_4}' \rightarrow \frac{p^3}{m} = \frac{c^3p^3}{fm} \qquad f = c^3 = h^{-6}$$

$$\underline{\psi}_5 = \frac{1}{p\omega^2} \rightarrow {\psi_5}' = \frac{1}{cph^2\omega^2} \qquad \underline{\psi}_5 = {\psi_5}' \rightarrow \frac{1}{p\omega^2} = \frac{1}{cph^2\omega^2} \qquad h = \sqrt{\frac{1}{c}}$$

$$\underline{\psi}_6 = \frac{E}{p} \rightarrow {\psi_6}' = \frac{jE}{cp} \qquad \underline{\psi}_6 = {\psi_6}' \rightarrow \frac{E}{p} = \frac{jE}{cp} \qquad j = c$$

$$\underline{\psi}_7 = \varepsilon \rightarrow {\psi_7}' = k\varepsilon \qquad \underline{\psi}_7 = {\psi_7}' \rightarrow \varepsilon = k\varepsilon \qquad k = 1$$

$$\underline{\psi}_8 = \frac{\eta p}{\omega m} \rightarrow {\psi_8}' = \frac{n\,\eta cp}{h\omega fm} \qquad \underline{\psi}_8 = {\psi_8}' \rightarrow \frac{\eta p}{\omega m} = \frac{n\,\eta cp}{h\omega fm} \qquad n = \frac{f\sqrt{\frac{1}{c}}}{c} = \frac{c^3h}{c} = c^2h$$

$$\underline{\psi}_9 = \frac{\dot{\varepsilon}}{\omega} \rightarrow {\psi_9}' = \frac{q\dot{\varepsilon}}{h\omega} \qquad \underline{\psi}_9 = {\psi_9}' \rightarrow \frac{\dot{\varepsilon}}{\omega} = \frac{q\dot{\varepsilon}}{h\omega} \qquad q = h$$

$$\underline{\psi}_{10} = \frac{P}{m\sqrt{p}} \rightarrow {\psi_{10}}' = \frac{sP}{fm\sqrt{cp}} \qquad \underline{\psi}_{10} = {\psi_{10}}' \rightarrow \frac{P}{m\sqrt{p}} = \frac{sP}{fm\sqrt{cp}} \qquad s = f\sqrt{c}$$

$$\underline{\psi}_{11} = \frac{V}{\sqrt{p}} \rightarrow {\psi_{11}}' = \frac{vV}{\sqrt{cp}} \qquad \underline{\psi}_{11} = {\psi_{11}}' \rightarrow \frac{V}{\sqrt{p}} = \frac{vV}{\sqrt{cp}} \qquad v = \sqrt{c}$$